PAPER

A study on coconut fatty acid diethanolamide-based polyurethane foams

Xuedong Leng,[a] Cong Li,[a] Xiaoxia Cai, [ID] *[a] Zhizhou Yang, [ID] [a] Fengshan Zhang,*[b] Yanshao Liu,[b] Guihua Yang,[a] Qiang Wang,[a] Guigan Fang[c] and Xian Zhang [ID] [a]

The possibility of using coconut fatty acid diethanolamide, a derivate from coconut oil as a bio-based polyol for the synthesis of polyurethane foam was explored. The intrinsic tertiary amine moiety in this polyol (p-CFAD) endowed an auto-catalytic effect in the synthesis process of polyurethane foams, combined with a shorter cream and gelation time compared to the fossil-based polyol 3152. H-nuclear magnetic resonance (^{1}H-NMR) and Fourier transform infrared spectrometry (FTIR) were conducted to characterize the chemical structural features of the p-CFAD, and rheology measurement showed the shear-thinning behavior due to the branched structure. A thermal conductivity comparable to the commercial rigid polyurethane foam was achieved when 40wt% fossil-based polyol 3152 was substituted with the bio-based p-CFAD. With the increased content of the p-CFAD, a transition of the physical properties from rigid PU foam to soft PU foam was observed. Scanning electron microscopy (SEM) revealed the occurrence of the interconnected pores on the cell walls with the increase of the added p-CFAD, implying the possibility of regulating the cellular structure and foam properties via the incorporation of the p-CFAD. Results showed the feasibility of using p-CFAD as a potential polyol in the development of bio-based polyurethane foams with high performance.

Introduction

As a multifunctional organic polymer material, polyurethane has a wide range of applications: rigid/soft foam, coatings, adhesives, sealants, elastomers, etc.[1,2] It has a wide range of terminal application markets.[3] Polyurethane foam, as one of the application forms of polyurethane, has been attracting attention because of its high porosity, low density and high strength.[4,5] As one of the important insulation materials in today's construction field, rigid polyurethane foam with an abundant closed-cell structure has good thermal insulation and superior weather resistance.[6] At the same time, it is also an important application material in the field of cold chain insulation.[7,8] As the research on polyurethane foam materials continues, its application fields are expanding, including household, transportation, aviation and other industries, thus putting higher demands on the performance of polyurethane foam.[9,10] In the production process of polyurethane foam, according to different application requirements, the polyol, isocyanate and catalyst types can be adjusted to produce different properties of foam, such as high temperature resistant foam, flame retardant foam, acoustic insulation foam, high resilience foam, etc.[11,12]

In the 21st century, with the rapid development of global industrialization, petrochemical resources are getting depleted, and problems such as serious petroleum-based pollution and difficulties in waste degradation have seriously affected the development of polyurethane industry.[13–16] Therefore, it is particularly important to find suitable alternatives for petroleum-based materials.[17] Within the field of polyurethane, finding suitable bio-renewable raw materials to replace petroleum-based polyols has become the focus of research.[18–21] With the intensive research on the high value of bio-based materials, plant oil has become the important research target for petroleum-based polyol alternatives due to its widely sources, low price, recyclability and convenient to production.[22] It has been found that bio-based polyols prepared from plant oils can effectively regulate the properties of polyurethane foams by replacing fossil-based polyols. Therefore, the application of plant oil as a renewable raw material to replace fossil-based polyols in the preparation of polyurethane foams is of research value and practical significance.[23–27]

Since coconut oil is a rich renewable resource that is largely cultivated in Asia and Africa, it is one of the most readily available plant oils and the preparation process is relatively simple.[28] In addition, the bio-based polyurethane foam made from coconut oil can replace the petroleum-based polyols to

[a] School of Materials Science & Engineering, State Key Laboratory of Biobased Material and Green Papermaking, Qilu University of Technology (Shandong Academy of Sciences), Jinan 250353, China. E-mail: cxx@qlu.edu.cn

[b] Hua Tai Group, Guangrao County, Dongying City, Shandong, China. E-mail: htjszx@163.com

[c] Key Lab. of Chemical Engineering of Forest Products, National Forestry and Grassland Administration, Nanjing 210042, China

a certain extent and has the property of recycling, which is beneficial to the protection of the environment.[28,29] At present, coconut oil-derived polyols are mostly obtained from the oxidation and subsequent hydroxylation of the unsaturated double bonds of the fatty acid chains, or from the trans-esterification with glycerol to monoglycerides.[30–32] It was noteworthy that as one of the valuable derivates of the coconut oil, though coconut fatty acid diethanolamide (CFAD) has been extensively applied as commercial emulsifier in daily life, the research of CFAD on the polyurethane foam synthesis is rarely conducted. Different from the hydroxylation or the trans-esterification approach, CFAD was obtained *via* the amidation of the coconut oil.[33] Distinct synthesis routes determine the chemical structure of the CFAD is quite different from the polyols derived from hydroxylation and the transesterification. Therefore, it is worthwhile to study the possibility of using CFAD as bio-based polyol for the polyurethane preparation.[34]

In this paper, bio-based polyurethane foams were synthesized by a one-step process through the purification of industrial coconut fatty acid diethanolamide (*p*-CFAD). The chemical structure and viscosity of the purified bio-based polyol were characterized. The catalytic effect of bio-based polyols was discussed by adjusting the proportion of *p*-CFAD to observe the creaming time and the gelation time. Detailed cellular structures were characterized *via* scanning electron microscopy (SEM) and the morphology transition with the increased content of the *p*-CFAD was investigated. Bio-based polyurethane foams prepared with different contents of the *p*-CFAD were successfully prepared, which demonstrated distinct thermal and physical properties, and the feasibility of using *p*-CFAD as a potential bio-based alternative to fossil-based polyols was studied carefully.

Experimental sections

Materials

Industrial grade coconut fatty acid diethanolamide is offered by Suzhou Rujie Chemical Industry Co., Ltd. Petrochemical polyol 3152 (315 mg per KOH per g)was purchased from Stepan Inc. Isocyanate (PAPI™ 27 Polymeric MDI) and silicone surfactants (VORASURF™ DC 5357) were supplied by Dow Chemical Inc. The commercial catalyst (Polycat®8 and Polycat® 5) was obtained by Air Products and Chemicals, Inc. Ethyl ether was supplied by Yantai YUANDONG Co., Ltd. Sodium bicarbonate was purchased from Shanghai Macklin Biochemical Technology Co., Ltd. Fig. 1 shows the schematic chemical structure of the three main raw materials.

Coconut fatty acid diethanolamide purification

The industrial grade coconut fatty acid diethanolamide was dissolved in ethyl ether with a volume ratio of 1 : 3, and 5 wt% bicarbonate solution was then added. The small amount of insoluble matter was removed *via* the separating funnel. The ethyl ether phase was further washed *via* the 5 wt% bicarbonate solution for 5 times. For each time, the upper layer was kept and washed by bicarbonate solution thoroughly. After that, the ethyl ether phase was transferred to a round bottom neck and evaporated under reduced pressure with a rotary evaporation at 50 °C for 6 h to remove the organic solvent. Subsequently, the temperature was raised to 100 °C and a reduced pressure of 0.1 MPa was applied for 5 h to evaporate the residual water in the system. Finally, a transparent yellow liquid was produced, which is the purified coconut fatty acid diethanolamide, denoted as *p*-CFAD.

Preparation of rigid polyurethane foam

The formulations used for the preparation of polyurethane foam were listed in Table 1. The isocyanate index for this study was 1.1. First of all, all materials (including foaming agent: water), except isocyanate, were added to the semicircular mold and mixed well. Then, the isocyanate was added into the mold, mixed with high-speed and free foaming, the cream time, mixing time and gel time were recorded. The mixing time of each foam was ensured to be as consistent as possible. Cured at room temperature for 7 days after foaming is completed. The prepared polyurethane foam samples were named according to the type and ratio of polyol as follows, 100% polyol 3152 – PU-3152, 60% polyol 3152 + 40% *p*-CFAD – PU-40-*p*-CFAD, 40% polyol 3152 + 60% *p*-CFAD – PU-60-*p*-CFAD, 20% polyol 3152 + 80% *p*-CFAD – PU-80-*p*-CFAD, 100% *p*-CFAD – PU-*p*-CFAD.

Characterization

Polyol characterization. The viscosity changes of petroleum-based polyols and bio-based polyols were measured by a Rheometer (ARES-G2) (TA Instruments, USA) at a shear rate of 0 to 100 1/s at 50 °C. ^{1}H-NMR spectra were produced on the AVANCE, II,400, Bruker (Germany) 600 MHz spectrometer. Samples were dissolved in Deuterated Chloroform (CDCl$_3$).[35] The *p*-CFAD was characterized for chemical structure by total reflection mode of Fourier transform infrared (FTIR) spectrometer at 500 ~ 4000 cm^{-1}. Molecular weight characteristics of petroleum-based polyols and bio-based polyols were characterized by Gel Permeation Chromatography (GPC).[36]

Foam characterization. All foam samples were matured at room temperature for at least seven days before being used for testing.

Foam cell structures were observed by scanning electron microscopy (ZEISS-G500, ZEISS Ltd, German) under 3 KV voltage conditions. A thin foam sample (5 × 5 mm) was gold-coated by evaporated gold for sputter coating, then cell structures was captured in cross-section perpendicular to the rising direction of the foam at 50× and 200× magnifications.[37] Then, with FIJI Image software, foam cell particle size was counted. The regularity of the foam cell structure is reflected by plotting the distribution of the counted cell pore sizes.[38] The foam was evaluated for chemical structure by total reflection mode of Fourier transform infrared (FTIR) spectrometer at 500 ~ 4000 cm^{-1}. FTIR spectra were collected by a Nexus 470 FTIR spectrometer (Nicolet, USA) in attenuated total reflectance mode with a subscale of 4 cm^{-1} and 16 scans for each sample.[39] The heat resistance of the foam was determined by thermogravimetric analyzer (TGA). The percentage weight loss of the
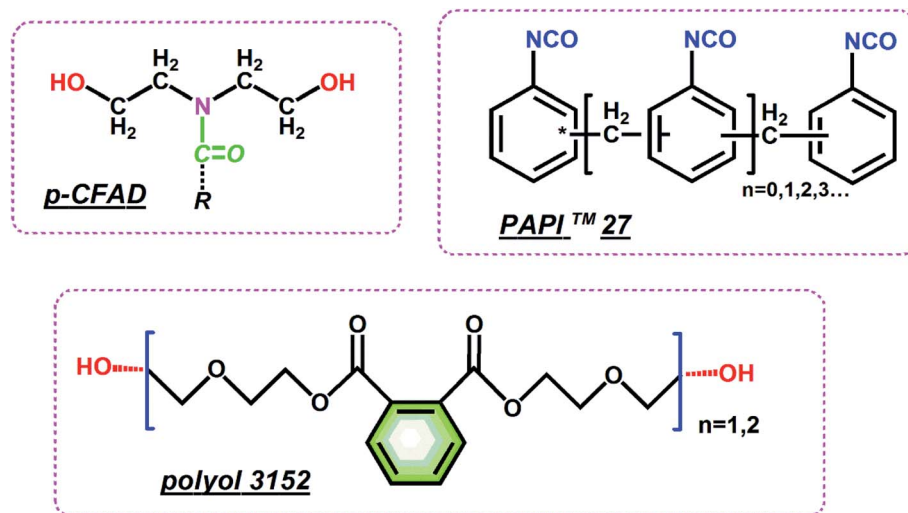
Fig. 1 Chemical structure formula of *p*-CFAD, polyol 3152 and PAPI™ 27.

samples (5 ~ 10 mg) was measured by TGA (Mettler, Switzerland) at a temperature range of 45 to 800 °C under a nitrogen atmosphere at a temperature rise rate of 10 °C min⁻¹.[40] Thermal transitions were measured *via* Differential Scanning Calorimetry (DSC Q 2000, TA Instruments) at a heating rate of 10 °C min⁻¹ (the sample weight was 5 ~ 10 mg). According to ASTM C518-2017, the thermal conductivity of foams was tested by a heat flow meter instrument (Laser Comp FOX 200, TA Instruments)(the sample size was 150 × 150 × 20 mm). In accordance with ISO 844-2007 compressive tests of the samples were carried out with a universal testing machine (WDW-50E) (Jinan Times Trial Gold Co., China). The foam sample of 10 × 10 × 10 mm in the direction of the foam rise was compressed to 90% of its initial height. The apparent density of the foams was measured according to ASTM D1622-2014.

Results and discussion

Structural features of *p*-CFAD

^{1}H-NMR spectrum of *p*-CFAD was presented in Fig. 2a. It can be seen that the proton signal shows multi peaks, which can be classified into five regions with respect to the chemical shift and are denoted as a, b, c, d and e, respectively. Region a located at around 5.3 ppm is correlated to the protons of double bonds;

region b (4 ~ 3.7 ppm) is correlated to the protons of hydroxyl groups; region c (3.7 ~ 2.8 ppm) corresponds to the protons of the methylene adjacent to the hydroxyl groups; region d (2.5 ~ 2 ppm) corresponds to the protons of the methylene adjacent to the nitrogen atoms, and region e (1.7 ~ 0.8 ppm) corresponds to the protons located on the fatty acid chains. A schematic reflecting the chemical structure feature of the *p*-CFAD is shown in Fig. 2a, in which the related typical protons are classified into 5 categories, *i.e.* a, b, c, d and e.

The infrared signal of *p*-CFAD was shown in Fig. 2b. Several chemical structural features of the *p*-CFAD can be recognized on the infrared spectrum. The obvious peak centered at 1621 cm⁻¹ is the characteristic signal of the amide group, which corresponds to the amide moiety existing in the *p*-CFAD. The hydroxyl groups at the chain end of the *p*-CFAD molecule was also reflected *via* the peak signal centered at 3346 cm⁻¹. Moreover, the fatty acid chain structure was revealed by the combined peaks located at 2919 cm⁻¹ and 2846 cm⁻¹.

In terms of molecular size, the comparison of *p*-CFAD and the commercial fossil-based polyol 3152 can be conducted *via* the GPC chromatography approach. Fig. 3a displays the different retention times between *p*-CFAD and the polyol 3152 *via* the GPC. The longer retention time of *p*-CFAD (peak at 24.66 min) indicates that compared to polyol 3152, *p*-CFAD possess

Table 1 Formulation with different substitution ratios of *p*-CFAD for polyurethane foam synthesis

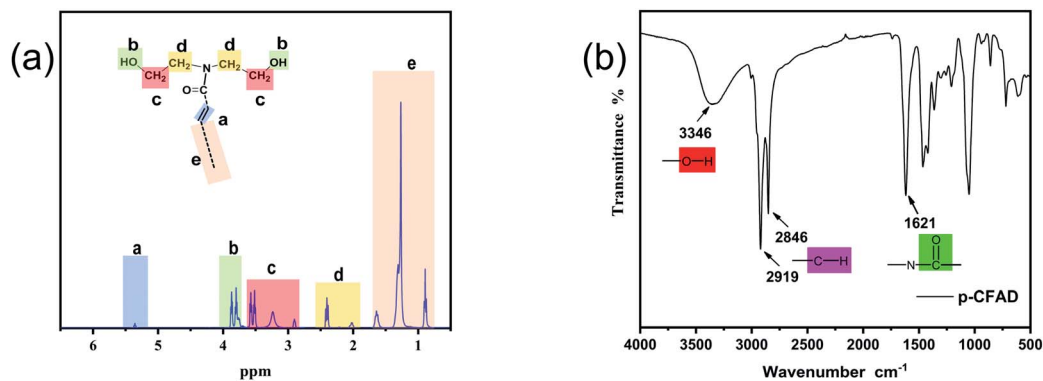| Foam formulation		0	20%	40%	60%	80%	100%
Polyol	3152	100	80	60	40	20	0
	p-CFAD	0	20	40	60	80	100
Catalyst	Polycat 5	0.64	0.64	0.64	0.64	0.64	0.64
	Polycat 8	0.42	0.42	0.42	0.42	0.42	0.42
Surfactant	Dabco DC 5357	2.5	2.5	2.5	2.5	2.5	2.5
Blowing agent	H₂O	3	3	3	3	3	3
Isocyanate	PAPI 27	124.64	136.36	140.17	143.98	147.79	151.61

Fig. 2 ^{1}H NMR Spectrum (a) and FTIR spectrum (b) of *p*-CFAD.

a relatively smaller molecular size. This result was further confirmed by the rheological behavior as shown in Fig. 3b. Compared to the polyol 3152, *p*-CFAD demonstrates remarkable lower viscosities in the entire shear frequency range. This is consistent with the longer retention time of *p*-CFAD observed in the GPC chromatography. Besides, it is noteworthy that a slight decline of viscosity occurred to *p*-CFAD in the initial frequency range. This is a shear-thinning phenomenon and mostly happens to materials with branch structures. As described in the ^{1}H-NMR section, the structure of pendent fatty acid chain in the *p*-CFAD molecule plays an important role in the shear-thinning, by which the entanglement among molecular chains can be reduced in the shear flow field. Therefore, it can be speculated that the incorporation of *p*-CFAD into the polyol 3152 would decrease the material viscosity and facilitate the mixing efficiency in the preparation of the polyurethane foam.

Polyurethane synthesis and properties

Table 1 exhibits the formulations for the polyurethane synthesis with different *p*-CFAD substitution ratios. The corresponding mixing time, cream time and gel time are shown in Fig. 4. It can be found from Fig. 4 that there is a remarkable decrease in cream time and gel time with the increase of the *p*-CFAD ratio in the whole system. This phenomenon can be attributed to the

intrinsic tertiary amine moiety existing in the *p*-CFAD, by which the reactions of isocyanates with water (blowing) and polyols (polymer gelation) can be catalyzed. Compared to the polyol 3152, this autocatalytic effect of *p*-CFAD endows a shorter cream and gelation time in the polyurethane foam synthesis process. The effect of the *p*-CFAD on the porous cell morphologies and the related properties of the foams have been studied in this work.

Fig. 5 shows the cross-sectional morphologies of the foams along the rising direction. Distinct cellular structures and morphologies were observed with the addition of the different content of *p*-CFAD in the PU system. Compared to the neat fossil-based PU foam, the PU-*p*-CFAD counterpart demonstrates a totally different cellular morphology. The SEM observation reveals that the internal structure of the PU-3152 comprises closed cells and the amount of open cells is small (Fig. 5a), whereas extensive interconnected pore cells were found in the PU-*p*-CFAD foam (Fig. 5d) and a partial enlarged image in Fig. 5d clearly demonstrated the detailed structures of these interconnected pore cells. The formation of these pores on the cell wall can be attributed to the relatively lower molecular weight of the *p*-CFAD. As is known, the polyurethane foaming is a complicated process including the gas bubble expansion and the urea/urethane chain propagation, in which polyol structure
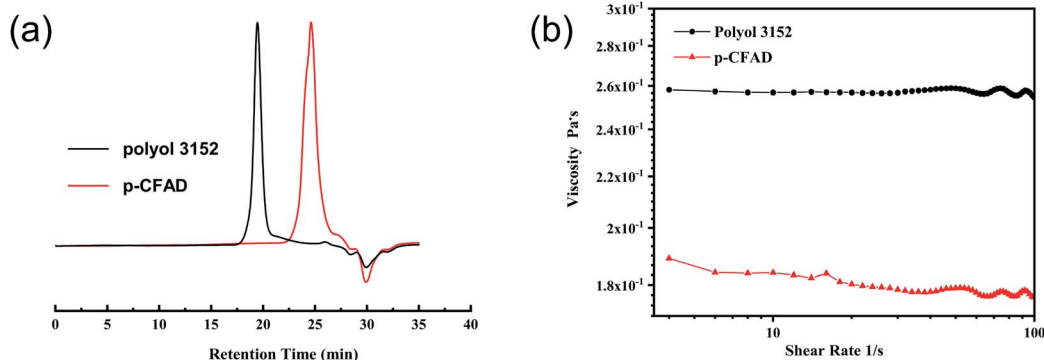

Fig. 3 (a) GPC chromatograms showing the retention times for 3152 and *p*-CFAD; (b) frequency dependence of the complex viscosities of the 3152 and *p*-CFAD at room temperature.
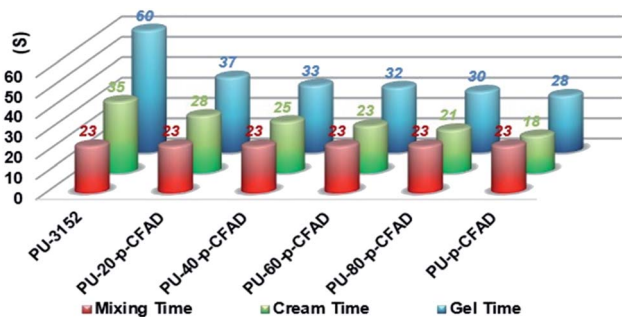
Fig. 4 Mixing time, cream time and gel time for the polyurethane foams synthesized with different *p*-CFAD substitution ratios.

plays an important role.[41] In terms of *p*-CFAD, the intrinsic tertiary amine moiety accelerated the reaction between water and isocyanate, promoting the expansion of gas bubble; on the other hand, the relatively shorter chain of *p*-CFAD decelerated the length propagation of the urethane chains, reducing the resistance strength of the cell walls to the bubble expansion. As a result, interconnected pores were formed on the cell walls as the Fig. 5d shown. With the content of the *p*-CFAD decreasing, these interconnected pores are becoming insignificant and almost invisible. It can be seen in Fig. 5b that the cells were mostly closed pore structure and interconnected pores were rarely found. In conclusion, *p*-CFAD plays an important role in regulating the cell morphology of the polyurethane foam. By means of proper incorporation of the *p*-CFAD into the poly-urethane system, a closed pore structure was maintained, whereas interconnected pore structure could be obtained when more content of *p*-CFAD was introduced.

Fig. 6 is the FTIR spectra of the PU foams with different contents of *p*-CFAD, revealing the internal structural feature from the molecular level. Compared to the PU-3152, it can be found in Fig. 6a that the signal peaks at 2922 cm^{-1} and 2850 cm^{-1} are getting more and more stronger with the increase of the *p*-CFAD content. These peaks are attributed to the methylene groups on the coconut fatty acid chains of the *p*-CFAD, and the increased signal can be observed with more content of polyol 3152 was substituted by *p*-CFAD. The signal brand ranging from 1750 ~ 1700 cm^{-1} corresponds to the urethane carbonyl groups, and as Fig. 6b shown, a significant peak around at 1712 cm^{-1} can be found. Moreover, it is note-worthy that a shoulder peak around at 1733 cm^{-1} was also recognized with the incorporation of the *p*-CFAD in the PU foam. The specific signal location of the urethane carbonyl is correlated directly to the hydrogen-bonded effect on it. Higher hydrogen-bonded effect will cause a lower signal position of the urethane carbonyl and *vice versa*. The occurrence of the shoulder peak (around at 1733 cm^{-1} as shown in Fig. 6b) indi-cated that a more disordered urethane segment was formed after the incorporation of the *p*-CFAD. One possible reason for this is that the pendent fatty acid chain of the *p*-CFAD resulted in difficulties in the regular arrangement of the urethane segments.

The thermal properties of the prepared polyurethane foams were investigated by DSC and TGA analyses. Significant thermal transition can be found at a temperature ranging from 50 to 100 °C for all samples in Fig. 7. This transition can be attributed the dissociation of the hydrogen bonds which occurs at the glass transition temperature of the urethane segments.[42] It can be found in Fig. 7 that the transition temperature moved to a higher temperature with the increased content of the *p*-CFAD. One possible reason is due to the content of isocyanate added
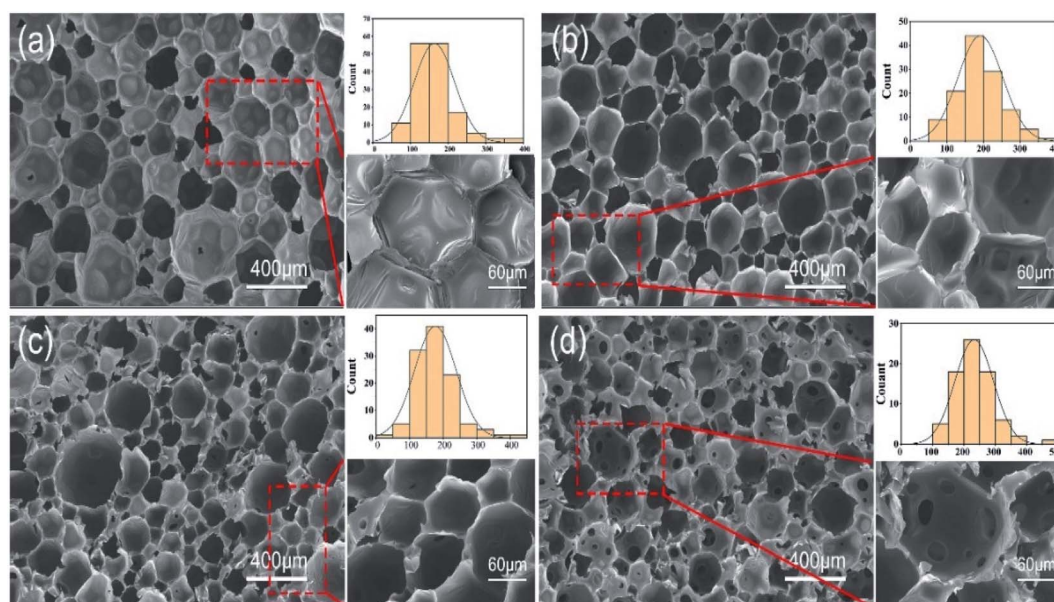

Fig. 5 (a) PU-3152 50×, 200× SEM images and cell size distribution; (b) PU-40-*p*-CFAD 50×, 200× SEM images and cell size distribution; (c) PU-80-*p*-CFAD 50×, 200× SEM images and cell size distribution; (d) PU-*p*-CFAD 50×, 200× SEM images and cell size distribution.
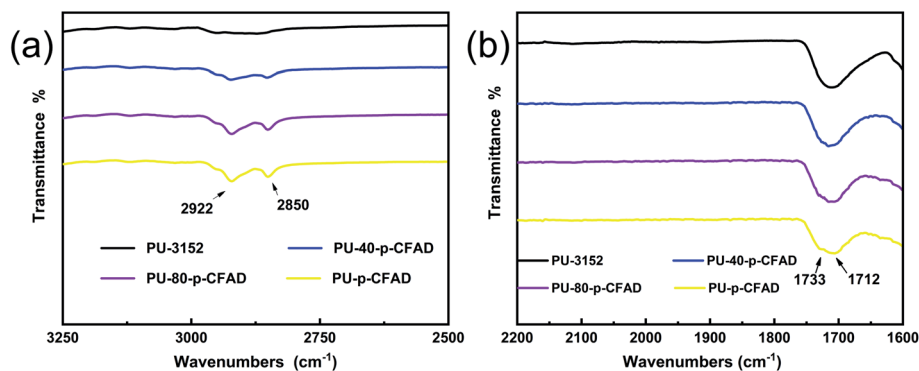
Fig. 6 FTIR spectra showing the methylene region (a) and urethane carbonyl region (b) for polyurethane foams.
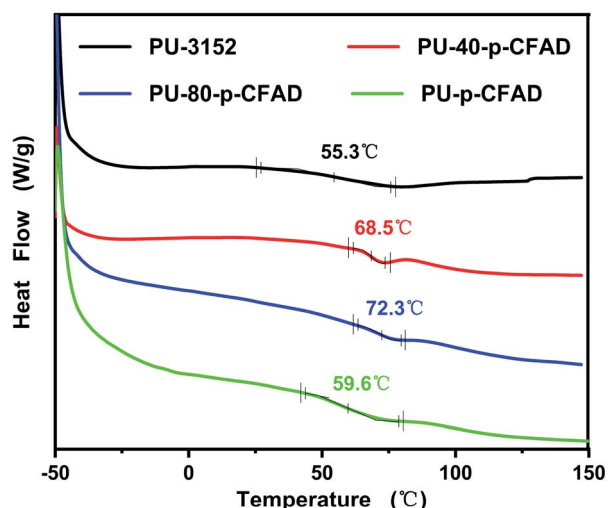

Fig. 7 DSC plot lines and thermal transition of PU foams.

into the system, the amount of which was increased combined with the added *p*-CFAD. The urethane segments were derived from the reaction of isocyanate and hydroxyl. Higher content of isocyanate would result in more amount of urethane segment, which would correspondingly favor the formation of hydrogen bonds and the increased thermal transition temperature. When polyol 3152 was totally substituted by *p*-CFAD, the thermal transition temperature shifted to a lower position again. This indicated that in addition to the amount of the urethane segment, the existence of the coconut fatty acid chain of the *p*-CFAD also play an important role in affecting the thermal transition temperature. It was speculated the pendent fatty acid chain of the *p*-CFAD could hinder the ordered arrangement of the urethane segments, which led to a decrease in the thermal transition temperature.[43]

The thermal degradation behaviors of the PU foams are described by TGA analysis. As Fig. 8 shows, there are two distinct degradation peaks for PU-3152. The first peak around at 310 °C mainly corresponds to the decomposition of urethane and allophanate bonds, and the second peak around at 435 °C mainly corresponds to the decomposition of polyol chains.[44,45]

Similar phenomenon occurs to PU-*p*-CFAD, in which two distinct degradation peaks located at around 230 °C and 500 °C can be recognized clearly. These two peaks are mainly related to the decompositions of the urethane and polyol segments, respectively. Compared to the urethane-related degradation peaks, the higher location in PU-3152 indicates that the urethane segments associated with the polyol 3152 possess a relatively higher thermal stability. In contrast, in terms of the poly-related degradation peak, PU-*p*-CFAD demonstrates a higher thermal stable performance. For the PU-40-*p*-CFAD and PU-80-*p*-CFAD samples, multiple degradation peaks can be distinguished in Fig. 8b and c, and the specific locations are listed in Table 2. Based on the TGA analyses of PU-3152 and PU-*p*-CFAD, it speculated that the multi-peak distribution is a combined effect of the poly 3152 and *p*-CFAD. In terms of PU-40-*p*-CFAD, the first peak T_1 and second peak T_2 are related to the *p*-CFAD and poly-3152 associated urethane segments, respectively. Whereas, the third peak T_3 and fourth peak T_4 are related to thepoly3152and *p*-CFAD associated soft segments, respectively. Similar case happens to the PU-80-*p*-CFAD sample and Table 2 shows the specific peaks of the decomposition temperatures.

The physical properties of the PU foams substituted with different contents of *p*-CFAD are listed in Table 3. It can be found the thermal conductivity of PU-40-*p*-CFAD is comparable to that of the PU-3152. Clearly, thermal insulation performance is directly related to the cell size and the closed-cell content.[46,47] As Fig. 5b shown, there is no obvious visible holes on the cell walls and the closed-cell structures are dominated for PU-40-*p*-CFAD. Therefore, a relatively good thermal insulation property can still be kept even when 40 wt% of the fossil-based polyol 3152 is substituted with the *p*-CFAD. With the increased content of the *p*-CFAD, the thermal conductivity increased as well, implying the thermal insulation performance is getting worse. As Fig. 5c and d shown, more interconnected pore cells were observed on the cell walls, which would facilitate the heat transfer through the cells and caused a decreased thermal insulation capacity. Moreover, the interconnected pore cells would affect the compression behaviors of the foams significantly.[48] As Table 3 shown, the compressive strength and modulus of compression for PU-*p*-CFAD are respectively over
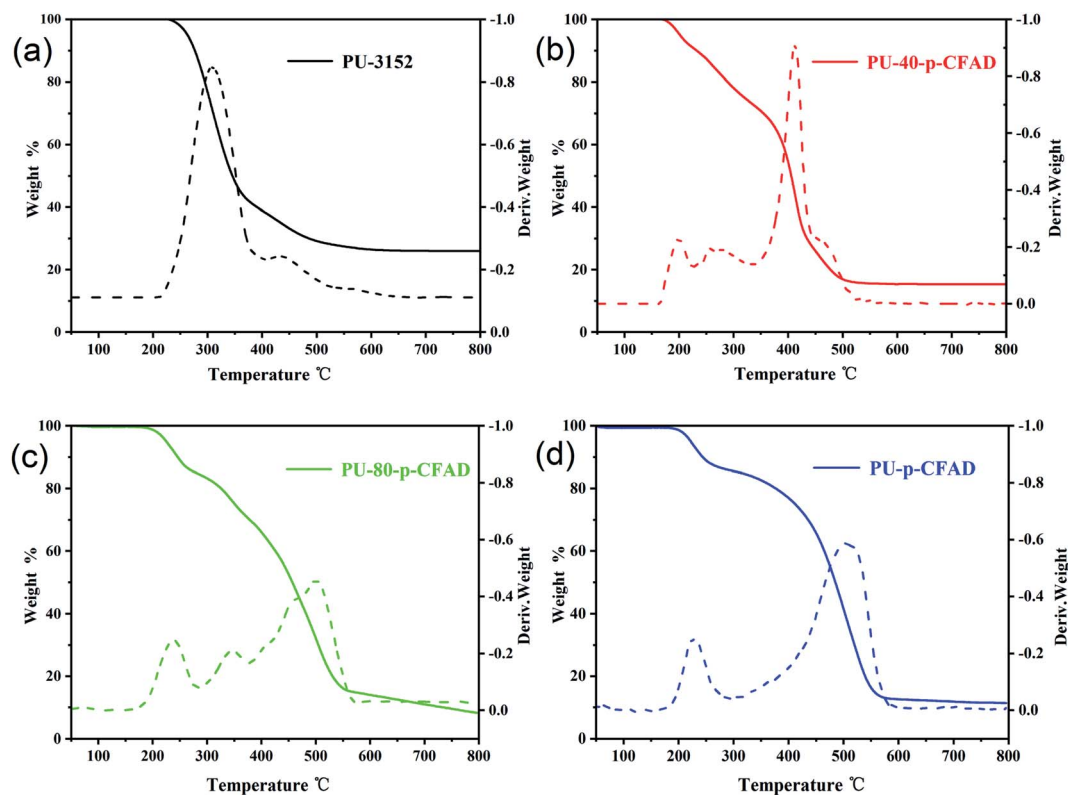
Fig. 8 DTG curves for polyurethane foam ((a) PU-3152, (b) PU-40-p-CFAD, (c) PU-80-p-CFAD, (d) PU-p-CFAD).

Table 2 The characteristic temperatures of thermal decomposition of the foams

Sample	Onset of degradation °C	T_1 °C	T_2 °C	T_3 °C	T_4 °C
PU-3152	216.5	310	435	—	—
PU-40-p-CFAD	175.33	199.6	270.5	412.1	463.8
PU-80-p-CFAD	166.6	235.3	344.5	458.4	500.7
PU-p-CFAD	160.1	227.5	505.1	—	—

two times and eight times lower than those of the PU-3152, showing a significantly softer touch relative to the PU-3152. Featured with the structure of extensive interconnected pore cells, the high content of p-CFAD incorporated foams demonstrated properties closer to the soft foam. It was concluded that the cellular structure and morphology of the PU foam can be regulated *via* controlling the content of the added p-CFAD,

whereby an effective transition from rigid PU foam to soft PU foam can be achieved.

Conclusions

In this work, the possibility of using coconut fatty acid diethanolamide as the alternative to fossil-based polyol was investigated. The chemical structural feature of p-CFAD was revealed *via* ^{1}H-NMR and FTIR, and the comparisons of the molecular weight and rheology behavior between p-CFAD and polyol 3152 were also conducted. Compared to the commercial polyol 3152, the intrinsic tertiary amine moiety in p-CFAD endows this material an unique autocatalytic effect, leading to a shorter cream and gelation time in the polyurethane foam synthesis process. Compared with other literature findings, combining the shear thinning properties of p-CFAD gives it potential for application in spraying. Detailed cellular structures and morphologies of the foams were characterized *via* SEM

Table 3 Characterization of physical and mechanical properties of foams

Properties	PU-3152	PU-40-p-CFAD	PU-80-p-CFAD	PU-p-CFAD
Thermal conductivity mW (mK^{-1})	26 ± 0.5	28 ± 0.5	45 ± 0.5	51 ± 0.5
Density (kg/m^3)	45.2 ± 1.3	41.2 ± 1.1	35.4 ± 0.8	32.1 ± 1.5
Compressive strength (kPa) (vertical to foam rise direction)	240 ± 20	198 ± 20	148 ± 20	95 ± 20
Modulus of compression (MPa)	2.4 ± 0.3	1.7 ± 0.2	0.8 ± 0.2	0.3 ± 0.2
Closed-cell content%	93	90	58	47

measurement. Interconnected pore cells were found with the increased addition of *p*-CFAD in the PU system, and a remarkable transition from rigid to soft foam was observed. The possible reason for the transition was discussed correspondingly. Compared to the neat poly-3152 based polyurethane foam, the PU-40-*p*-CFAD demonstrated a comparable thermal conductivity, showing a potential in the application of heat insulation. While with the increase of the added *p*-CFAD, the appearance of the open cells featured with the interconnected pores on the cell walls changed the mechanical properties of the foams significantly, and a property closer to semi-rigid foam was found. This is a different result compared to other literature. The discovery of this property implies that *p*-CFAD has great potential for the preparation of sound-absorbing and vibration-damping materials. Though the optimization and utilization of *p*-CFAD in the PU foam synthesis are still changes, the success in foaming process and the unique properties show its promising potential as the building block for the development of bio-based polyurethane foams.

Author contribution

Conceptualization, C. L.; data curation, C. L., X. L., Z. Y., F. Z., Y. L., G. Y., Q. W., X. Z. and G. F.; formal analysis, Z. Y. and Y. L.; funding acquisition, C. L., X. C. and Z. Y; methodology, C. L. and X. L.; writing – original draft, C. L. and X. L.; writing – review and editing, X. C. All authors have read and agreed to the published version of the manuscript.

Conflicts of interest

The authors declare there are no conflicts of interest.

Acknowledgements

References

1 D. E. Heath, S. A. Guelcher and S. L. Cooper, in *Biomaterials Science*, Elsevier, 2020, pp. 103–107.

2 B. Eling, Ž. Tomović and V. Schädler, *Macromol. Chem. Phys.*, 2020, **221**, 2000114.

3 N. V. Gama, A. Ferreira and A. Barros-Timmons, *Materials*, 2018, **11**, 1841.

4 Z. Tongtong, C. Shuming, Z. Wenbo, W. Yebin and Y. Jiang, *Mater. Sci.*, 2019, **25**, 85–89.

5 A. Prociak, L. Szczepkowski, J. Ryszkowska, M. Kurańska, M. Auguścik, E. Malewska, M. Gloc and S. Michałowski, *J. Polym. Environ.*, 2019, **27**, 2360–2368.

6 C. A. Ikutegbe and M. M. Farid, *Renewable Sustainable Energy Rev.*, 2020, **131**, 110008.

7 J. Andersons, M. Kirpluks, L. Stiebra and U. Cabulis, *Mater. Des.*, 2016, **92**, 836–845.

8 H. Beneš, A. Paruzel, O. Trhlíková and B. Paruzel, *Eur. Polym. J.*, 2017, **86**, 173–187.

9 T. A. Phung Hai, M. Tessman, N. Neelakantan, A. A. Samoylov, Y. Ito, B. S. Rajput, N. Pourahmady and M. D. Burkart, *Biomacromolecules*, 2021, **22**, 1770–1794.

10 P. K. S. Pillai, M. C. Floros and S. S. Narine, *ACS Sustainable Chem. Eng.*, 2017, **5**, 5793–5799.

11 R. Dhoke, A. Ojha, A. K. Chaudhary and R. Vijayakumar, *Cell. Polym.*, 2021, **40**, 73–86.

12 V. Jonjaroen, S. Ummartyotin and S. Chittapun, *Algal Res.*, 2020, **51**, 102057.

13 A. Svärd, R. Moriana, E. Brännvall and U. Edlund, *ACS Sustainable Chem. Eng.*, 2018, **7**, 790–801.

14 J. C. Gomez, R. Zakaria, M. M. Aung, M. N. Mokhtar and R. B. Yunus, *J. Mater. Res. Technol.*, 2020, **9**, 16303–16316.

15 E. Watt, M. Picard, B. Maldonado, M. A. Abdelwahab, D. F. Mielewski, L. T. Drzal, M. Misra and A. K. Mohanty, *RSC Adv.*, 2021, **11**, 21447–21462.

16 A. Alassali, W. Calmano, E. Gidarakos and K. Kuchta, *RSC Adv.*, 2020, **10**, 44989–44996.

17 X.-Z. Wang, M.-S. Lu, J.-B. Zeng, Y. Weng and Y.-D. Li, *Green Chem.*, 2021, **23**, 307–313.

18 T. A. P. Hai, N. Neelakantan, M. Tessman, S. D. Sherman, G. Griffin, R. Pomeroy, S. P. Mayfield and M. D. Burkart, *Green Chem.*, 2020, **22**, 3088–3094.

19 K. Nomura and N. W. Binti Awang, *ACS Sustainable Chem. Eng.*, 2021, **9**, 5486–5505.

20 H. Li, N. Mahmood, Z. Ma, M. Zhu, J. Wang, J. Zheng, Z. Yuan, Q. Wei and C. C. Xu, *Ind. Crops Prod.*, 2017, **103**, 64–72.

21 M. Bachmann, A. Kätelhön, B. Winter, R. Meys, L. J. Müller and A. Bardow, *Faraday Discuss.*, 2021, **230**, 227–246.

22 P. Furtwengler, R. Matadi Boumbimba, A. Sarbu and L. Avérous, *ACS Sustainable Chem. Eng.*, 2018, **6**, 6577–6589.

23 P. Appaiah, L. Sunil, P. Prasanth Kumar and A. Gopala Krishna, *J. Am. Oil Chem. Soc.*, 2014, **91**, 917–924.

24 M. Kurańska and A. Prociak, *Ind. Crops Prod.*, 2016, **89**, 182–187.

25 S. Suryani, S. Sariani, F. Earnestly, M. Marganof, R. Rahmawati, S. Sevindrajuta, T. M. I. Mahlia and A. Fudholi, *Processes*, 2020, **8**, 402.

26 A. M. Patil, H. D. Jirimali, V. V. Gite and R. N. Jagtap, *Prog. Org. Coat.*, 2020, **149**, 105895.

27 M. Borowicz, J. Paciorek-Sadowska and M. Isbrandt, *Ind. Crops Prod.*, 2020, **155**, 112831.

28 W. He, P. Kang, Z. Fang, J. Hao, H. Wu, Y. Zhu and K. Guo, *Ind. Eng. Chem. Res.*, 2020, **59**, 17513–17519.

29 B. J. Rashmi, D. Rusu, K. Prashantha, M. F. Lacrampe and P. Krawczak, *J. Appl. Polym. Sci.*, 2013, **128**, 292–303.

30 P. Shankar, S. Ahuja and A. Tracchio, *Agro Food Ind. Hi Tech*, 2013, **24**, 62–64.

31 F. Liu and S. Chen, *J. Polym. Environ.*, 2021, 1–14.

32 D. Ji, Z. Fang, W. He, Z. Luo, X. Jiang, T. Wang and K. Guo, *Ind. Crops Prod.*, 2015, **74**, 76–82.

33 S. Xu, M. E. Lamm, M. A. Rahman, X. Zhang, T. Zhu, Z. Zhao and C. Tang, *Green Chem.*, 2018, **20**, 1106–1113.

34 M. A. Sawpan, *J. Polym. Res.*, 2018, **25**, 1–15.

35 A. Fröscher, K. Langenbach, E. von Harbou, W. R. Thiel and H. Hasse, *Ind. Eng. Chem. Res.*, 2019, **58**, 5622–5630.

36 H. Li, Y. Zhong, X. Lai, X. Li, P. Chen and X. Zeng, *J. Adhes. Sci. Technol.*, 2015, **29**, 740–752.

37 X. Zhou, M. M. Sain and K. Oksman, *Composites, Part A*, 2016, **83**, 56–62.

38 F. Liu and D. Han, *J. Appl. Polym. Sci.*, 2011, **121**, 1536–1542.

39 E. Kustiyah, D. S. Putra, D. Gerry, D. F. Firdaus and M. Chalid, *Macromol. Symp.*, 2020, **391**, 1900153.

40 S. Bhoyate, M. Ionescu, P. K. Kahol, J. Chen, S. R. Mishra and R. K. Gupta, *J. Appl. Polym. Sci.*, 2018, **135**, 467–473.

41 R. Mort, K. Vorst, G. Curtzwiler and S. Jiang, *RSC Adv.*, 2021, **11**, 4375–4394.

42 R. W. Seymour and S. L. Cooper, *Macromolecules*, 1973, **6**, 48–53.

43 L.-S. Teo, C.-Y. Chen and J.-F. Kuo, *Macromolecules*, 1997, **30**, 1793–1799.

44 R. Tanaka, S. Hirose and H. Hatakeyama, *Bioresour. Technol.*, 2008, **99**, 3810–3816.

45 P. Parcheta, E. Głowińska and J. Datta, *Eur. Polym. J.*, 2020, **123**, 109422.

46 P. Buahom, C. Wang, M. Alshrah, G. Wang, P. Gong, M.-P. Tran and C. B. Park, *Nanoscale*, 2020, **12**, 13064–13085.

47 M. Kurańska, K. Polaczek, M. Auguścik-Królikowska, A. Prociak and J. Ryszkowska, *Polymer*, 2020, **190**, 122164.

48 A. H. Shaik, S. Banerjee, A. Rahaman, S. Agashe, A. Khan and M. R. Chandan, *J. Polym. Res.*, 2021, **28**, 1–9.